Available online at www.sciencedirect.com
SCIENCE DIRECT®
Computational Materials Science 36 (2006) 42–48
COMPUTATIONAL MATERIALS SCIENCE
www.elsevier.com/locate/commatsci

Beyond the point defect limit: Simulation methods for solid solutions and highly disordered systems

N.L. Allan [a,*], G.D. Barrera [b], M.Yu. Lavrentiev [c,1], C.L. Freeman [a], I.T. Todorov [d], J.A. Purton [d]

[a] School of Chemistry, University of Bristol, Cantock's Close, Bristol BS8 1TS, UK
[b] Departamento de Química, Universidad Nacional de la Patagonia SJB, Ciudad Universitaria, (9000) Comodoro Rivadavia, Argentina
[c] EURATOM/UKAEA Fusion Association, Culham Science Centre, Oxfordshire OX14 3DB, UK
[d] CLRC, Daresbury Laboratory, Warrington, Cheshire WA4 4AD, UK

Received 14 July 2004; accepted 2 December 2004

Abstract

We discuss how two techniques, based on (1) lattice statics/lattice dynamics simulations and (2) Monte Carlo methods may be used to calculate the thermodynamic properties of solid solutions and highly disordered systems. The lattice statics/lattice dynamics calculations involve a full free-energy structural optimization of each of a number of configurations, followed by thermodynamic averaging. The Monte Carlo simulations include the explicit interchange of cations and use the semigrand canonical ensemble for chemical potential differences. Both methods are readily applied to high pressures and elevated temperatures without the need for any new parameterization; at agreement between the two techniques is better at high pressures where anharmonic terms are smaller. Vibrational contributions to thermodynamic quantities of mixing are examined. A range of examples, including binary oxides, garnets and carbonates, are used to illustrate the methods.

Keywords: Solid solutions; Disorder; Simulation; Garnets; Entropy

1. Introduction

Grossly disordered minerals and non-ideal solid solutions, continue to present considerable challenges to the theoretician. The cluster variation method (CVM) [1], for example, widely used for metallic alloys, often performs poorly where species involved are markedly dissimilar, as is usually the case in ceramics and minerals. Using parameterized Hamiltonians (e.g., of Ising type) is increasingly difficult beyond binary alloys. Disorder in ionic materials has often been studied via point defect calculations (the dilute limit). Another route has been via the use of a 'supercell' [2], in which a periodic 'superlattice' of defects is introduced, extending throughout the macroscopic crystal; an artificial ordering is thus imposed on the arrangement of defects by the periodic boundary conditions. In this paper we discuss two multi-configuration techniques for solid solutions or disordered systems with a *finite* impurity or defect content far from the dilute limit. Both of these, unlike the point defect or supercell calculations, sample many different arrangements of ions. Both are readily applied to high pressure and include thermal (vibrational) effects, which have proved problematic for traditional methods [1].

The first of these builds on an efficient method for the fully dynamic structure optimisation of large unit cells

* Corresponding author. Tel.: +44 117 9288308; fax: +44 117 9256012.
E-mail address: n.l.allan@bris.ac.uk (N.L. Allan).
[1] On leave from Institute of Inorganic Chemistry, 630090 Novosibirsk, Russia.

0927-0256/$ - see front matter © 2005 Elsevier B.V. All rights reserved.
doi:10.1016/j.commatsci.2004.12.083

which uses lattice statics and quasiharmonic lattice dynamics (QLD). The accurate calculation of the free energy via QLD is quick and computationally efficient and does not resort to lengthy thermodynamic integration. The full set of free energy first derivatives is calculated analytically and a *full* minimisation of the free energy with respect to all structural variables for large unit cells is possible [3]. Here this technique is extended to evaluate the *free energies* of solid solutions and phase diagrams at *any* pressure. This is achieved by forming a thermodynamic average of the free energies of a number of configurations. No a priori assumptions are made regarding the configurational entropy contribution; vibrational contributions to thermodynamic quantities at any temperature and pressure are determined straightforwardly. This configurationally averaging differs in some important respects from CVM [4], which defines the energy of the system as an expansion of effective cluster interactions (ECIs). These ECIs are calculated by fitting to the energy of several optimized configurations. A large range of further configurations can then be generated by applying the ECIs within the configuration to calculate their energy. Where the interactions within the system are complex or long-range the number of ECIs that need to be defined in the CVM can make the expansion unfeasible [5]. Generally calculations using CVM do not take the effect of relaxation or vibration into account. The use of quasirandom structures (QRS) allows an estimate of the vibrational contributions [6] and very recently Wu et al. [7] have proposed the use of bond-length dependent force constants to allow for relaxation. Application of CVM to ionic systems such as perovskites [8] and carbonates [9] has proved problematic.

The second technique we use in this paper is the well-known Monte Carlo method, implemented in such a way that *both* the atomic configuration *and* the atomic coordinates of all the atoms are changed (Monte Carlo Exchange (MCX)). Absolute values of the free energy cannot be obtained readily from Monte Carlo simulations. Nevertheless, the semigrand canonical ensemble [10] provides a convenient route to accurate chemical potential *differences* accurately and hence the phase diagram. All calculations reported here use widely used interatomic potential models within the framework of an ionic model.

2. Thermodynamics of solid solutions: theoretical methods

2.1. Lattice statics and dynamics

In principle a solid solution can assume any state in which each atom can be at any position. The only states of practical importance away from the melting point will lie at the bottom of K local minima in the energy of the system, i.e., they correspond to a given configuration. For each configuration k, we suppose there exists a number of states which correspond to small or moderate changes in the internal and external lattice strains. Using the label $k = 1, \ldots, K$ for the configuration, then the enthalpy and Gibbs energy in the isobaric–isothermal (NPT) ensemble are given by [11]

$$H = \frac{\sum_{k=1}^{K} H_k \exp(-G_k/k_B T)}{\sum_{k=1}^{K} \exp(-G_k/k_B T)} \tag{1}$$

$$G = -k_B T \ln \sum_{k=1}^{K} \exp(-G_k/k_B T) \tag{2}$$

G_k is the Gibbs energy for the *relaxed* structure of each possible cation arrangement. We thus have expressions for any thermodynamic quantity in terms of thermodynamic quantities obtained with particular configurations. The thermodynamic averaging is performed over the results of a set of full free-energy minimisations of different arrangements (configurations) of the cations within a supercell.

For other than the smallest supercells it is impractical to sum over all K configurations and all summations in Eqs. (1) and (2) are restricted to K' configurations chosen at random. K in the second term of Eq. (3) is replaced by K' and

$$H = \frac{\sum_{k=1}^{K'} H_k \exp(-G_k/k_B T)}{\sum_{k=1}^{K'} \exp(-G_k/k_B T)}, \quad \text{and} \tag{3}$$

$$G = -k_B T \ln K - k_B T \ln \left(\sum_{k=1}^{K'} \exp(-G_k/k_B T)/K' \right) \tag{4}$$

2.2. Monte Carlo simulations

The Monte Carlo exchange simulations (MCX) [12] are carried out within the NPT ensemble. Randomly selected atoms are moved at random in order to take vibrational effects into account. At any step, a random choice is made whether to attempt a random exchange between two atoms, a random displacement of an ion, or a random change in the volume of the simulation box with relative probabilities 1:N:1. To determine whether the change is accepted or rejected, the usual Metropolis algorithm is applied. The maximum changes in the atomic displacements and the lattice parameters are governed by the variables r_{max} and v_{max}, respectively, and these are adjusted automatically during the equilibration part of the simulation to maintain an acceptance/rejection ratio of $\approx$0.3. Calculation of the free energy is less straightforward than with QLD; semigrand canonical ensemble simulations are used to calculate the difference in chemical potential of ions A and B.

The conversion of one species, B into another, A, is considered, and the resulting potential energy change $\Delta U_{B/A}$ determined. This is related to the change in chemical potential $\Delta\mu_{B/A}$ by,

$$\Delta\mu_{B/A} = -k_B T \ln \left\langle \frac{N_B}{N_A + 1} \exp(-\Delta U_{B/A}/k_B T) \right\rangle \qquad (5)$$

Every fifth step of the MCX simulation we evaluate the energy associated with the conversion of a randomly chosen ion type B to ion type A, $\Delta U_{B/A}$ and as the simulation proceeds the average value of the exponential in equation is determined.

3. Results

3.1. MnO–MgO

We start with the solid solution MnO–MgO. Shown in Fig. 1 are values of ΔH_{mix} at 1000 K and zero pressure, calculated using QLD and MCX for a 50/50 mixture with a unit cell of 128 atoms and 12,870 randomly chosen configurations. In the QLD all external and internal degrees of freedom are optimized for every configuration; for a detailed study of the convergence properties with cell size and number of arrangements, see Ref. [13]. The MCX simulations used a simulation cell of 512 ions, and 4×10^7 steps, following initial equilibration of 1×10^7 steps. The plot shows there is good agreement between QLD and MCX, despite QLD using vastly less configurations than MCX and neglecting higher-order anharmonic terms (though quantum effects are incorporated in QLD). The calculated ΔH_{mix} at 1000 K is symmetric with a maximum of 5.4 kJ mol^{-1}. No symmetry constraints are applied in any of the calculations. We have examined previously [11] the striking failure of mean-field approach and 'hybrid' potentials

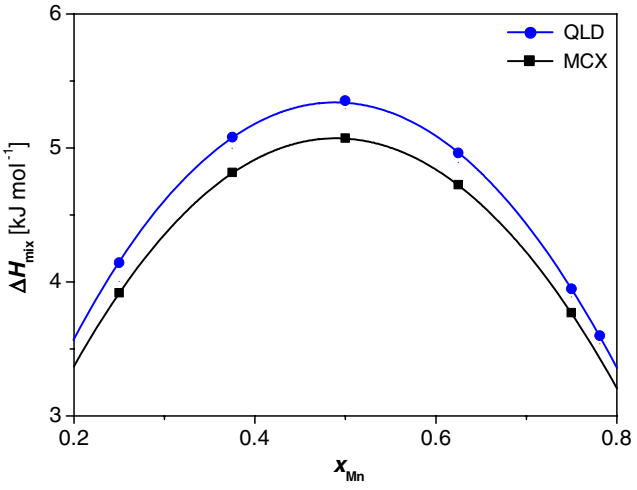

Fig. 1. ΔH_{mix} (kJ mol^{-1}) at 1000 K for MnO–MgO as a function of composition calculated using configurational QLD and using MCX.

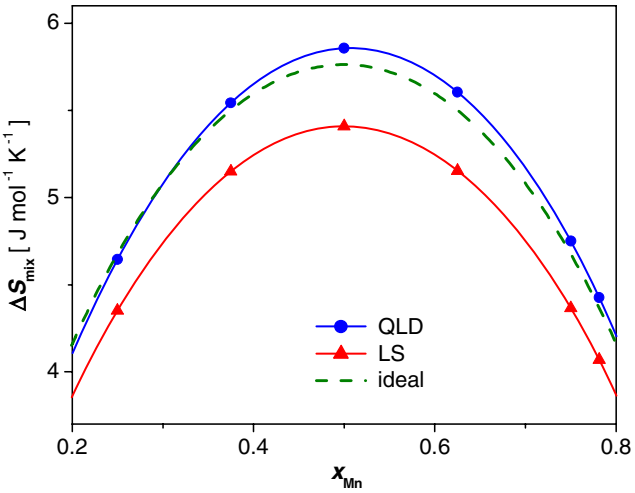

Fig. 2. ΔS_{mix} (J K^{-1} mol^{-1}) at 1000 K for MnO–MgO as a function of composition calculated using QLD (filled circles). The points (triangles) labeled LS are values calculated using configurational averaging but with each configuration minimized in the static limit. For comparison the ideal entropy of mixing is also shown (dashed line).

for ΔH_{mix}. Entropies of mixing, ΔS_{mix} calculated using QLD, include *both* configurational *and* vibrational entropies. Fig. 2 plots ΔS_{mix} as a function of composition at 1000 K. Note ΔS_{mix} is larger than the ideal value for compositions for $x_{Mn} > 0.25$.

The calculation of the free energy of mixing is a severe test of our model since ΔH_{mix} and $-T\Delta S_{mix}$ are often very close in magnitude. For MnO–MgO in the QLD, 250 configurations with a supercell of 128 atoms are sufficient to ensure adequate convergence in the positions of the two minima in the ΔG_{mix} vs. composition curves. It is *vital* to allow for atomic relaxation, as demonstrated strikingly in Fig. 3 which compares calculated

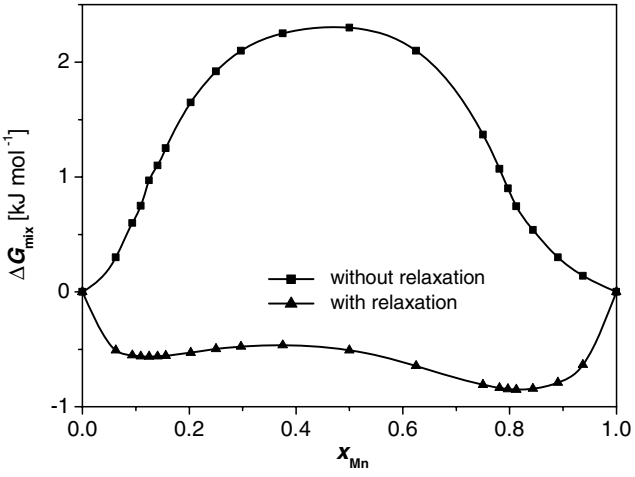

Fig. 3. Variations of ΔG_{mix} (kJ mol^{-1}) at 1000 K for MnO–MgO with composition, with and without relaxation are plotted. The difference between the two curves demonstrate the importance of atomic relaxation. All calculations are QLD.

ΔG_{mix} vs. composition curves at 1000 K with and without relaxation. In the absence of relaxation ΔG_{mix} is *positive* for all compositions studied.

Monte Carlo simulations at a given temperature in the semigrand canonical ensemble yield the calculated variation of $\Delta\mu_{Mg/Mn}$ with composition. As in the Margules approximation, we write the excess (non-ideal) free energy as a third degree polynomial in the concentration. The chemical potential difference then consists of an ideal solution term and a second degree polynomial. The results for $\Delta\mu$ at each temperature were fitted to such a polynomial. Integration gives the variation of free energy with composition, and these ΔG_{mix} vs. composition curves are similar to those obtained using the optimized QLD energies in Fig. 3. There is also good agreement between ΔS_{mix} values obtained via the Monte Carlo free energy and enthalpy of mixing and those obtained from QLD. From the temperature variation of ΔG_{mix} it is straightforward to calculate the phase diagram, as in Ref. [13].

It is computationally much cheaper to optimize every configuration in the static limit, using lattice statics (LS) and replacing G_k by H_k (static) in Eqs. (1)–(4). The vibrational contribution to H_k and the vibrational entropy S_k are ignored. Only *one* set of runs over the composition scale is required for *all* temperatures. The curve labelled LS in Fig. 2 shows ΔS_{mix} calculated using this approximation. The difference between the QLD and LS values represents the vibrational contribution (denoted using the subscript 'vib'). Neglecting effects due to thermal expansion, the LS values of ΔS_{mix} represent the configurational contribution to these quantities. The LS values of ΔS_{mix} are lower and smaller than the ideal entropy of mixing at all compositions. The configurational entropy of mixing is thus smaller than the ideal and the positive vibrational terms contribute to the *effective* ideality of the solid solution. The maximum contribution of $\Delta S_{mix(vib)}$ at 1000 K is 8% of the total ΔS_{mix} for $x_{Mn} = 0.5$. The contribution of $\Delta S_{mix(vib)}$ to the entropy of mixing of CaO–MgO solid solutions is much larger [12] due to the larger size-mismatch involved between the two cations.

3.2. Garnets

Aluminosilicate garnets ($X_3Al_2Si_3O_{12}$, X = Mg^{2+}, Ca^{2+}, Fe^{2+}, Mn^{2+}) form one of the most important solid solution minerals in the Earth's crust and upper mantle. We have chosen to perform an MCX study of two representative garnet binaries, pyrope (X = Mg)–grossular (X = Ca) and pyrope–almandine (X = Fe). The pyrope–grossular system presents particular complications due to the large difference in ionic radius between Ca^{2+} and Mg^{2+} and a configurational bias technique [12] was used to increase the number of successful interchanges. The simulations used a cell of 1280 ions containing 64 formula units, and 2.5×10^7 steps, following initial equilibration of 5×10^6 steps.

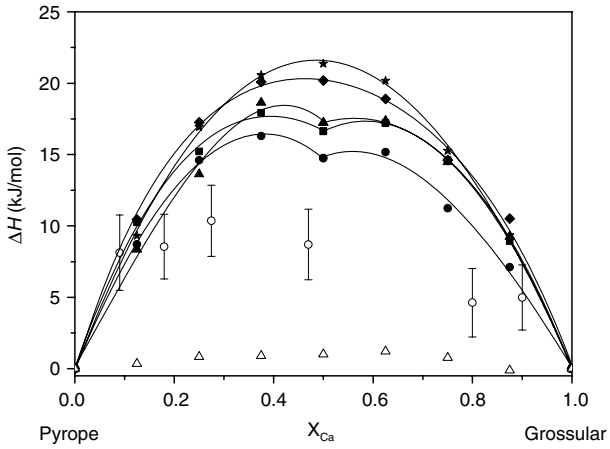

Fig. 4. ΔH_{mix} along the pyrope–grossular join. Calculated values are at $T = 1500$ K, pressure $P = 0$ (circles), 3 GPa (squares), 5 GPa (triangles), 10 GPa (diamonds), 15 GPar (stars). Experimental data (at $P = 0$) [3] are open circles. For comparison, ΔH_{mix} along the pyrope–almandine join (open triangles) is also shown.

For Py–Gr solid solutions we plot ΔH_{mix} at 1500 K and pressures from zero to 15 GPa in Fig. 4. These are all positive with a dip at lower pressures at a composition of ≈50:50, possibly hinting at a preferential ordering of Ca^{2+} and Mg^{2+}. Available experimental data [14] are also shown. These like the calculated values are positive and show similar asymmetry, with higher values for pyrope-rich garnets. Nevertheless quantitative agreement is rather poor. To some extent this can be related to large uncertainties in the calorimetric measurements. For example, three measurements of the enthalpy of pure end member pyrope differ by up to 2.4 kJ/mol [14]. Also shown in Fig. 4 is the analogous calculated ΔH_{mix} at 1500 K for Py–Alm at zero pressure. These values are all positive but much smaller than those for Py–Gr, as might be expected given the smaller size mismatch between Mg^{2+} and Fe^{2+}. We suggest that an experimental re-examination of the enthalpy of mixing of Py–Gr and Py–Alm is highly desirable.

In Fig. 5, calculated excess volumes for Py–Gr are compared with experiment. ΔV_{mix} is large and positive, as observed experimentally [15,16]. These results are in better quantitative agreement with experiment than those for ΔH_{mix} although in general on the high side and possibly less asymmetric. It is important to bear in mind again that experimental uncertainties are large. In contrast to the results for Py–Gr, volumes of mixing along the Py–Alm join are small (between 0 and 0.05 cm^3/mol). This agrees with Ref. [17] which concludes experimental data are indistinguishable from ideal.

In order to investigate how the atomic scale behaviour of the garnet solid solutions influences the thermodynamic properties, we have studied the short-range

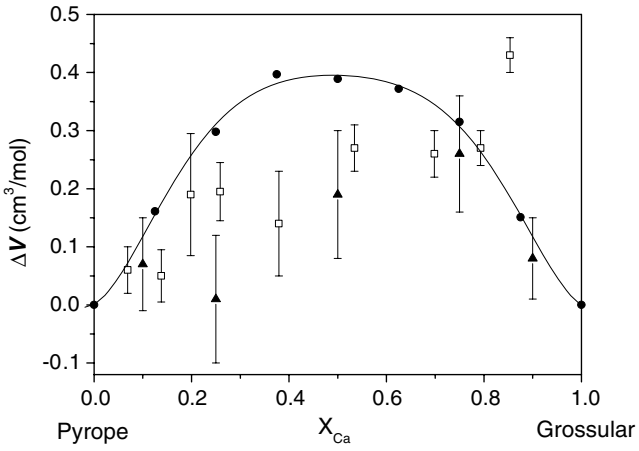

Fig. 5. ΔV_{mix} along the pyrope–grossular join. Calculations ($T = 1500$ K, zero pressure): solid circles, experiment ($T = 295$ K, zero pressure): [4]: empty squares, [5]: solid triangles.

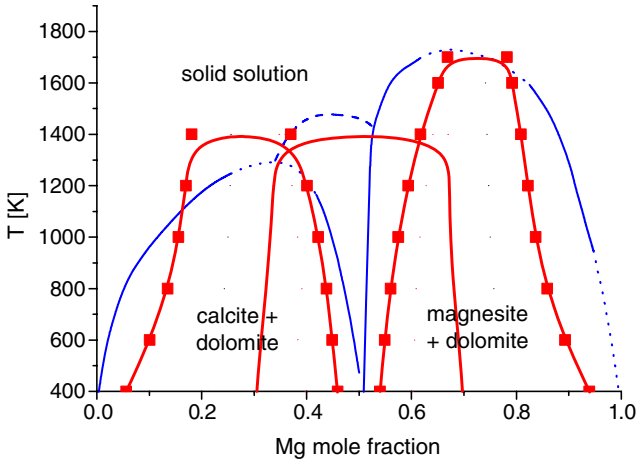

Fig. 6. Phase diagram for dolomite. Calculated results are squares (red). The blue line, i.e. the line which does not connect the sqaures, shows the experimental results, with the dotted line an extrapolation of the available experimental data. (For interpretation of the reference in colour in this figure legend, the reader is referred to the web version of this article.)

Ca–Mg ordering in Py–Gr garnets. Previous experimental ^{29}Si MAS MNR studies [18,19] together with computational results [20,21] concluded that the strongest cation interaction is that between dodecahedral sites linked via an edge-shared tetrahedron, i.e., between third nearest cation neighbours. We have monitored in our MCX simulations the nature of the third neighbour interactions in $Py_{50}Gr_{50}$ and $Py_{50}Alm_{50}$ as a function of temperature. Py–Alm behaves essentially as an ideal solution, with a random distribution of third neighbours. The Py–Gr solid solution is very different in that at low temperatures there are very few Mg–Mg (and Ca–Ca) third neighbour pairs. At higher pressures the number of Mg–Mg third nearest neighbour pairs increases in the Py–Gr solution. This is consistent with the different compressibilities of the Mg and Ca dodecahedral sites, with the Ca site more easily compressible and thus making the Mg and Ca sites more similar at higher pressures. This is also associated with the disappearance of the small dip in the composition variation of the enthalpies of mixing at higher pressures (Fig. 4) and the decrease of the enthalpy of mixing with increasing pressure.

3.3. Carbonates

Carbonates contribute a significant portion of the Earth's crust but have proved experimentally challenging [22] making them an ideal candidate for simulation. Computationally modelling of carbonates has had mixed success; the use of Lippmann Diagrams [23,24] proved problematic. We have attempted to model dolomite, the most abundant carbonate, using cheap potential methods [25] and preliminary results are presented here. Dolomite, $Ca_xMg_{(1-x)}(CO_3)_2$, has a hexagonal structure with planes of cations (Ca or Mg) separated by planes of carbonates.

Our calculations used a 72-cation unit cell (total atom number 360) over a range of compositions. All our calculations use LS and approximately 25,000 configurations. In Fig. 6, we present the calculated phase diagram of dolomite. The agreement with experiment is encouraging, with reproduction of all the main features. The main differences lie close to the end members and in large part are artefacts of the cell size used.

4. Final remarks

Solid solutions of ionic compounds have traditionally proved problematic for the theoretician. We have presented a range of methods for the simulation of such solid solutions, the accurate calculation of thermodynamic quantities of mixing, and also for the calculation of phase diagrams. No empirical data for the particular system under study are required. All the methods sample many configurations, explicitly considering different arrangements of ions, and allow for the *local* structural relaxation surrounding each cation. This relaxation is crucial. If ignored, the energy of exchange of any two ions is usually very high and all exchanges are rejected, thus sampling only one arrangement. All the methods include vibrational effects and are applicable over ranges of pressure and temperature. Disorder problems are often tackled by using a general Ising model, simplified by limiting interactions to a short range and a finite number of multi-site couplings. Such an approach is awkward to parameterize for ionic solids, where relaxation is crucial, and to apply over a range of pressures and temperatures. It is not readily generalised to less symmetric structures, to which we also wish to apply

the general methodology outlined here. In our methodology, no assumptions are made as to the nature of the solid solution.

In particular, we have demonstrated how the rapid calculation of the free energy via quasiharmonic lattice dynamics can be used to calculate thermodynamic properties of solutions over wide ranges of pressure and temperature including ΔH_{mix}, ΔS_{mix} and phase diagrams. Results compare well with those from Monte Carlo simulations in the semigrand canonical ensemble. Agreement is better at higher pressure [14] where internuclear distances are smaller and anharmonic contributions smaller. Quantum effects are included in the vibrational contributions at low temperatures. Calculated entropies of mixing include *both* configurational and vibrational contributions. For the latter we have seen when extrapolation from the point defect limit fails. The technique is limited by the accuracy of the quasiharmonic approximation, which breaks down with increasing amplitude of vibration and hence at high T, typically around two-thirds of the melting point for oxides.

The Monte Carlo and the configurational averaging methods each have their own strengths and advantages. Monte Carlo techniques are applicable to the solid at high temperatures and to melts [12]. The semigrand canonical ensemble is an attractive route to differences in chemical potential and consequent calculation of the free energy and the phase diagram. QLD is efficient and gives the free energies to high precision. Further work is in progress to develop all of the methods. We have also used similar techniques to examine trace element partitioning between minerals and melts [26] and applied QLD methods to highly non-stoichiometric compounds, such as oxygen-deficient perovskites [27]. In this case the relative energies of the configurations also have important consequences for the ion transport suggesting collective mechanisms are lower in energy than conventional single-jump mechanisms [26].

Acknowledgments

This work is funded by EPSRC grant GR/R85952. Computational facilities were made available through two JREI HEFCE grants. Help from Hugh Barron is gratefully acknowledged.

References

[1] D. de Fontaine, Cluster approach to order–disorder transformations in alloys, Solid State Phys. 47 (1994) 33–176.
[2] M.B. Taylor, G.D. Barrera, N.L. Allan, T.H.K. Barron, W.C. Mackrodt, Free energy of formation of defects in polar solids, Faraday Discuss. 106 (1997) 377–387.
[3] M.B. Taylor, G.D. Barrera, N.L. Allan, T.H.K. Barron, Free-energy derivatives and structure optimization within quasiharmonic lattice dynamics, Phys. Rev. B 56 (1997) 14380–14390.
[4] J.M. Sanchez, F. Ducastelle, D. Gratias, Generalized cluster description of multicomponent systems, Physica A 128 (1984) 334–350.
[5] A. van de Walle, G. Ceder, The effect of lattice vibrations on substitutional alloy thermodynamics, Rev. Mod. Phys. 74 (2002) 11–45.
[6] A. Zunger, S.-H. Wei, L.G. Ferreira, J.E. Benard, Special quasirandom structures, Phys. Rev. Lett. 65 (1990) 353–356.
[7] E.J. Wu, G. Ceder, A. van de Walle, Using bond-length-dependent transferable force constants to predict vibrational entropies in Au–Cu, Au–Pd, and Cu–Pd alloys, Phys. Rev. B 67 (2003) 134103.
[8] R. McCormack, B.P. Burton, Modeling phase stability in $A(B_{1/3}B'_{2/3})O_3$ perovskites, Comput. Mater. Sci. 8 (1997) 153–160.
[9] B.P. Burton, A. van de Walle, First-principles-based calculations of the $CaCO_3$–$MgCO_3$ and $CdCO_3$–$MgCO_3$ subsolidus phase diagrams, Phys. Chem. Miner. 30 (2003) 88–97.
[10] D. Frenkel, B. Smit, Understanding Molecular Simulation, second ed., Academic Press, SanDiego, London, 2002.
[11] N.L. Allan, G.D. Barrera, R.M. Fracchia, M.Yu. Lavrentiev, M.B. Taylor, I.T. Todorov, J.A. Purton, Free energy of solid solutions and phase diagrams via quasiharmonic lattice dynamics, Phys. Rev. B 63 (2001) 094203.
[12] M.Yu. Lavrentiev, N.L. Allan, G.D. Barrera, J.A. Purton, Ab initio calculation of phase diagrams of ceramics, J. Phys. Chem. B 105 (2001) 3594–3599.
[13] I.T. Todorov, N.L. Allan, M.Yu. Lavrentiev, C.L. Freeman, C.E. Mohn, J.A. Purton, Simulation of mineral solid solutions at zero and high pressure using lattice statics, lattice dynamics and Monte Carlo methods, J. Phys. Condens. Matter 16 (2004) S2751–S2770.
[14] R.C. Newton, T.V. Charlu, O.J. Kleppa, Thermochemistry of high-pressure garnets and clinopyroxenes in system CaO–MgO–Al_2O_3–SiO_2, Geochim. Cosmochim. Acta 41 (1977) 369–377.
[15] J. Ganguly, W. Cheng, H.St.C. O'Neil, Syntheses, volume, and structural-changes of garnets in the pyrope–grossular join—implications for stability and mixing properties, Am. Mineral. 78 (1993) 583–593.
[16] A. Bosenick, C.A. Geiger, Powder X-ray diffraction study of synthetic pyrope–grossular garnets between 20 and 295 K, J. Geophys. Res. 102 (1997) 22649–22657.
[17] C.A. Geiger, A. Feenstra, Molar volumes of mixing of almandine–pyrope and almandine–spessartine garnets and the crystal chemistry and thermodynamic-mixing properties of the aluminosilicate garnets, Am. Mineral. 8 (1997) 571–581.
[18] A. Bosenick, C.A. Geiger, T. Schaller, A. Sebald, A ^{29}Si MAS NMR and IR spectroscopic investigation of synthetic pyrope–grossular garnet solid-solutions, Am. Mineral. 80 (1995) 691–704.
[19] A. Bosenick, C.A. Geiger, B.L. Phillips, Local Ca–Mg distribution of Mg-rich pyrope–grossular garnets synthesized at different temperatures revealed by ^{29}Si MAS NMR spectroscopy, Am. Mineral. 84 (1999) 1422–1432.
[20] A. Bosenick, M.T. Dove, C.A. Geiger, Simulation studies on the pyrope–grossular garnet solid solution, Phys. Chem. Miner. 27 (2000) 398–418.
[21] W. van Westrenen, N.L. Allan, J.D. Blundy, M.Yu. Lavrentiev, B.R. Lucas, J.A. Purton, Dopant incorporation into garnet solid solutions a breakdown of Goldschmidt's first rule, Chem. Commun. 786–787 (2003).
[22] L.S. Land, Failure to precipitate dolomite at 25 °C from dilute solution despite 1000-fold oversaturation after 32 years, Aquat. Geochem. 4 (1998) 361–368.
[23] H. Gamsjäger, E. Königsberger, W. Preis, Lippmann diagrams: theory and application to carbonate systems, Aquat. Geochem. 6 (2000) 119–132.

[24] M. Prieto, A. Fernádez-González, U. Becker, A. Putnis, Computing Lippmann diagrams from direct calculation of mixing properties of solid solutions: application to the barite–celestite system, Aquat. Geochem. 6 (2000) 133–146.
[25] D.K. Fisler, J.D. Gale, R.T. Cygan, A shell model for the simulation of rhombohedral carbonate minerals and their point defects, Am. Mineral. 85 (2000) 217–224.
[26] C.E. Mohn, N.L. Allan, C.L. Freeman, P. Ravindran, S. Stølen, Collective ionic motion in oxide fast-ion-conductors, Phys. Chem. Chem. Phys. 6 (2004) 3052–3055.
[27] E. Bakken, N.L. Allan, T.H.K. Barron, C.E. Mohn, I.T. Todorov, S. Stølen, Order–disorder in grossly non-stoichiometric $SrFeO_{2.5}$ a simulation study, Phys. Chem. Chem. Phys. 5 (2003) 2237–2243.